Unraveling the mechanism of the NO reduction by CO on gold based catalysts

ARTICLE *in* JOURNAL OF CATALYSIS · MAY 2012

Impact Factor: 6.92 · DOI: 10.1016/j.jcat.2012.01.010

3 AUTHORS:

José Luis Cagide Fajín
University of Porto
43 PUBLICATIONS **474** CITATIONS
SEE PROFILE

Natália D. S. Cordeiro
University of Porto
245 PUBLICATIONS **3,049** CITATIONS
SEE PROFILE

José R B Gomes
University of Aveiro
188 PUBLICATIONS **2,568** CITATIONS
SEE PROFILE

Journal of Catalysis 289 (2012) 11–20

Contents lists available at SciVerse ScienceDirect

Journal of Catalysis

journal homepage: www.elsevier.com/locate/jcat

Unraveling the mechanism of the NO reduction by CO on gold based catalysts

José L.C. Fajín [a], M. Natália D.S. Cordeiro [a], José R.B. Gomes [b,*]

[a] REQUIMTE, Faculdade de Ciências, Universidade do Porto, P-4169-007 Porto, Portugal
[b] CICECO, Departamento de Química, Universidade de Aveiro, 3810-193 Aveiro, Portugal

ARTICLE INFO

Article history:
Received 14 October 2011
Revised 6 January 2012
Accepted 14 January 2012
Available online 3 March 2012

Keywords:
Heterogeneous catalysis
Gold surface
NO reduction
CO oxidation
Adsorption
Density functional theory
Hydrogenation

ABSTRACT

Periodic density functional theory (DFT) calculations have been used to unravel the mechanism of the NO reduction by CO ($NO + CO \rightarrow N_2 + CO_2$) on clean and hydrogen covered gold based catalysts. The effects caused by the presence of low-coordinated atoms on the catalyst were taken into consideration by using the stepped Au(3 2 1) surface. A careful analysis of several reaction mechanisms was made and it is concluded that if hydrogen species are not available on the catalyst surface, the N–O bond cleavage will proceed through the ON_2O and N_2O intermediates while CO reacts directly with formed oxygen adatoms. If hydrogen species are available on the catalyst, the reaction will occur via the NOH and N_2O intermediates. However, the reaction has to compete with a more favorable route, where NH_3 instead of N_2 is obtained after formation of NOH and NH_xOH intermediates. The calculations agree also with the experimental observation of the NCO intermediate species which is formed without energy cost from combination of CO and N fragments. The NCO species is very probably a spectator at moderate temperatures since its evolution toward N_2 and CO_2 is less favorable than other possible routes studied in this work. Finally, calculated reaction rate constants at three different temperatures show that most of the reactions studied are only possible at moderately high temperature.

1. Introduction

The increasing concerns with the greenhouse effect have led to more restrictive rules related to the exhaust gas emissions, as can be corroborated by the *Emission Standards* for the different pollutant gases produced for road vehicles in Europe [1]. Among these pollutant gases, nitrogen oxides (NO_x) and in particular nitrous oxide (N_2O, warming potential 310 times larger than that of CO_2 gas and 15 times than that of CH_4) are under rigorous control [2]. The reduction of these NO_x species follows two generic reaction schemes named *Selective Catalytic Reduction* (SCR) [3] and *NO_x Storage-Reduction* (NSR) [4,5]. The SCR method consists in the direct reduction of the NO_x species on the catalyst and is commonly employed in stationary NO_x sources, needing a reducing agent, which can be urea, ammonia, or hydrocarbons from the fuel. The NSR method is composed by two cycles, where the combustion in the engine occurs under long oxygen-rich or short fuel-rich periods. In the former regime, the NO_x species are captured and stored, while in the fuel-rich cycle, the NO_x species are reduced to N_2 (catalysts built from a pure noble metal or from bimetallic alloys including a noble metal). In general, the catalysts used in the NO_x reduction are constituted by a noble metal(s) and a support [6,7], which can be based on Ru [8], Rh [9], Ir [10–12], Pd [13–15], Pt [16–22], Au [23–26], Ag [27–30], or alloys of these metals with cheaper metals [8,9,20,22,31,32], but there are some exceptions, where the noble metal was successfully replaced by other elements [33–37].

Several mechanisms were proposed for the reduction of NO_x oxides on catalysts based on noble metals dispersed on supports, since different intermediates have been observed in the course of the catalytic reactions depending on the experimental conditions and on the catalyst's nature. One of the central reactions for the NO_x reduction is the NO reaction with CO (i.e., $NO + CO \rightarrow \frac{1}{2}N_2 + CO_2$). The desirable product containing nitrogen atoms is gaseous N_2 but formation of N_2O as a side product is also possible with the consequent environmental implications exposed above [2]. Therefore, important efforts are being made to optimize the catalysts in such a way that formation of the latter species is avoided [19,31,38,39]. Due to the importance of the N_2O species on the reaction of NO_x reduction and in order to simplify the systems being studied, some works focus only on the direct reduction of N_2O to molecular nitrogen [10,17,29,40].

Very recent work shows that the reaction of NO_x reduction is not that simple and different mechanisms are being proposed according to new observations. For example, different reaction intermediaries were observed during the nitrogen oxides removal reaction on alumina-supported silver [41], on titania-supported gold [42,43], and on ceria-alumina-supported gold catalysts [44]. Within these works, the formation of an isocyanate intermediate

* Corresponding author. Fax: +351 234 401 470.
E-mail address: jrgomes@ua.pt (J.R.B. Gomes).

0021-9517/$ - see front matter © 2012 Elsevier Inc. All rights reserved.
doi:10.1016/j.jcat.2012.01.010

(NCO) was observed evidencing signs of N–O bond dissociation leading to N and O adatoms on the catalysts surfaces; the former adatoms eventually will react with CO. Importantly, Thibault-Starzyk et al. suggested also C–O bond dissociation and formation of CN species adsorbed on the noble metal of the Ag/Al_2O_3 catalyst [41]. However, it seems that the identification of the surface species in the course of the NO_x reduction reaction is not trivial or it is strongly influenced by the experimental working conditions. In fact, the NCO intermediate was not found by Debeila et al. [45–48] in their DRIFTS analysis on the adsorption of NO on Au/TiO_2. Importantly, depending on the pretreatment of the catalyst, Debeila et al. observed the formation of dinitrosyl complexes attached to the same Au atom ($Au(NO)_2$ species were found either in the presence or in the absence of CO [45,46]), or the formation of nitrates and nitrites (only when CO was absent [47,48]). Recent DFT studies on the unsupported model Au(1 1 1) surface suggest the formation of $(NO)_2$ dimers due to the high activation energy barrier for the NO dissociation on that gold surface [49] and subsequent formation of N_2O species. All of the previous experimental and computational results imply different possible reaction routes for the NO reduction with CO on noble metal based catalysts.

The cleavage of the N–O bond seems to be the crucial step during NO reduction by CO on several different catalysts [13,43,50–52]. The NO dissociation can lead to the formation of N_2O, through reaction of dissociated N atoms with undissociated NO molecules [21,38,53,54], or to the formation of NCO, through reaction of dissociated N atoms with CO [43,51,52]. Based also on previous studies, other reaction routes are also possible for the initial steps of NO reduction in the presence of CO, namely, direct reaction of the NO fragments in the $Au(NO)_2$ complexes to yield N_2O without needing previous N–O bond cleavage [45,46]. These reaction routes were investigated by Vinod et al. [55] for the NO adsorption on the stepped Au(3 1 0) surface. They conclude that routes based on previous NO dissociation are more plausible. This is at least surprising since the dissociation of the NO molecule does not seem to be an easy process on surfaces of less reactive noble metals such as gold (energy barrier for NO dissociation on the Au(1 1 1) surface is 3.9 eV [49]). However, much smaller reaction barriers are possible if promoters are available on the catalytic surface. In fact, very recently we explored alternative routes for the NO dissociation considering the Au(3 2 1) surface as a model catalyst, and found that the presence of H atoms on the gold catalyst was able to reduce importantly the energy required to dissociate the NO species [56], which is in agreement with experimental work, where at moderate temperatures the NO reduction starts only if hydrogen is available [52,57,58]. Interestingly, at high temperatures, the presence of hydrogen on the catalyst inhibits the NO reduction with CO, suggesting that direct reaction of NO with CO is more favorable [52] but some steps of the NO reduction by CO, e.g., NO dissociation, were found to be structure sensitive [21,51,59–65].

From what has been written above, there are still many controversial points about the mechanism of the NO reduction with CO on noble metal based catalysts. Many of the mechanistic studies on the nitrogen oxides removal reaction considered gold as the noble metal in the catalyst (and also copper and silver), most probably due to the enhanced stability and unexpected catalytic behavior of gold in the oxidation of CO. Herewith, we try to shed light on the reaction of NO reduction by CO. For that purpose, DFT calculations were performed for several different possible reaction steps that may be present in this reaction using the Au(3 2 1) surface as a model of the active phase in a gold containing catalyst. The (3 2 1) Miller index was found to be the most active for NO bond scission in the case of Rh [66] and it allows to consider the effects of low-coordinated atoms at the surface steps, which were found to be very important in several different catalytic reactions [56,67–69]. In fact, highly dispersed gold nanoparticles supported on different oxides were suggested previously as effective catalysts for the NO reduction with CO, suggesting a crucial role of the low-coordinated atoms in the catalysis of this reaction [70].

2. Computational details

2.1. Slab model

The infinite Au(3 2 1) surface and its interactions with the different species implied in the NO + CO reaction were modeled using the three-dimension (3D) periodic-slab approach. The positions of the gold atoms in the stepped Au(321) surface were obtained in a previous work [68]. The metal slab has 15 gold atoms per unit cell distributed in four atomic layers parallel to the (1 1 1) terraces. A vacuum region of at least 10 Å thick was introduced between repeated cells in the z direction as required to build a surface for use with the 3D VASP code [71–73]. This unit cell consists in a monoclinic prism with the angles between the x and z axis and between the y and z axis of exactly 90° and the angle between the x and y axis being different from 90°. Further, in this crystal system, the vectors x, y, and z have different lengths and the Au–Au bond distances are of 2.9161 Å [68]. This stepped surface has a considerable variety of possible adsorption positions including positions on (or near to) low-coordinated gold atoms, as shown in Fig. 1. The different possible hollow sites are labeled in Fig. 1 with a, b, c, d, e, f, g, h, and i letters while the top sites are labeled with 1, 2, 3, and 4 numbers. The nomenclature for the bridge positions, which are not illustrated in Fig. 1, is as follow: a letter b followed with the numbers of the two nearest-neighbor gold atoms, ordered from the right of the slab to the left and from the positions closer to the reader to those farther. Furthermore, as in previous works [69], the uppermost seven of the fifteen gold atoms of the slab (constituting the $Au(3\,2\,1)^S$ face) were fully relaxed during the calculations.

2.2. Adsorption and transition state configurations

The (co-)adsorption energies and geometries of the adsorbates on the Au(3 2 1) surface were obtained from DFT calculations. The PW91 generalized gradient approach (GGA) exchange correlation potential [74] and the projected augmented-wave (PAW) method as implemented in VASP [75,76] were considered here. The cutoff used for the plane waves expansion was 415 eV and a grid of $7 \times 7 \times 1$ Monkhorst–Pack special k-points [77] was used for the numerical integration in the reciprocal space, a combination that was found to be enough for energy and geometry convergence. The geometry of the adsorbates and the atomic positions in the two uppermost metallic layers were fully relaxed using the conjugate–gradient (CG) algorithm.

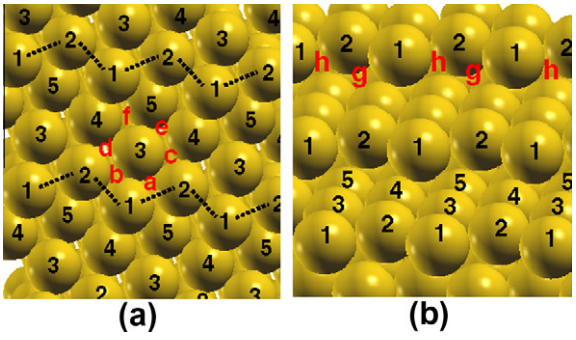

Fig. 1. (a) Top and (b) side views of possible adsorption sites on the Au(3 2 1) surface. Letters and numbers are used to label hollow and top positions, respectively. See text for additional details.

The localization of the transition state (TS) structures for all the reaction steps on the Au(3 2 1) surface was carried out using the Dimer approach [78]. The convergence criteria for the total energy change and for the forces acting in the ions were 10^{-6} eV and 10^{-3} eV/Å, respectively. These quite strict criteria are necessary in TS searches on the stepped surfaces to avoid that the algorithm converges to local minima. Computation of a single imaginary frequency for the configurations obtained with the Dimer method ensured that those were true TS structures. In most cases, visual inspection of the vibrational mode corresponding to the imaginary frequency was enough to ascertain that the TS structures connected the desired reaction states. When the connection was not obvious, reaction coordinates (reverse and forward directions) were followed for checking if the TS structures were connecting the proposed reactants and products states.

In this work, (co-)adsorption energies, activation energy barriers, and reaction energies were corrected with the *zero point vibrational energy* (ZPVE) using the harmonic oscillator approach. In the case of single species adsorbed onto the surface, i.e., N_2, O_2, N_2O, CO, N, NH, NH_2, NH_3, H_2, H_2O, NO_2, NH_2OH, OH, CO_2, NO, NOH, NHOH, and NCO, the adsorption energy (E_{ads}) was calculated as:

$$E_{ads} = E_{slab-adsorbate} - E_{slab} - E_{adsorbate} \quad (1)$$

where E_{slab} refers to the total energy of the slab model representing the Au(3 2 1) surface, $E_{adsorbate}$ to the gas-phase total energy of the corresponding adsorbate computed by placing it in a sufficiently large box, and $E_{slab\text{-}adsorbate}$ refers to the total energy of the slab-adsorbate system. In the case of co-adsorbed species, i.e., N + CO, N + N, NO + NO (ONOO), N_2O + O, N + NO, N_2 + O, N_2O + CO, N_2 + CO_2, NO + CO, NO + O, NH_2 + OH, NHOH + H, NH_2OH + H, NH_3 + OH, N + H, NH + H, NH_2 + H, N + CO_2, NCO + NO, N_2O + CO, NCO + N, N_2 + CO, O + H, H + H, N + O, OH + H, N + OH, NH + OH, NOH + H, NO + H, N + H_2O, CO + O, CO + O_2 (OCOO), CO_2 + O, O + O, CO + OH (OCOH), CO_2 + H, OCOH + OH, and CO_2 + H_2O, the co-adsorption energy ($E_{co\text{-}ads}$) was calculated as:

$$E_{co-ads} = E_{slab-(frag1+frag2)} - E_{slab} - E_{frag1} - E_{frag2} \quad (2)$$

where E_{slab} refers to the total energy of the slab model representing the Au(3 2 1) surface, $E_{frag1(frag2)}$ stands for the gas-phase total energy of a fragment, and $E_{slab\text{-}(frag1+frag2)}$ refers to the total energy of the slab-(frag1 + frag2) system. Finally, according to these equations, negative values of E_{ads} ($E_{co\text{-}ads}$) mean favorable adsorption (co-adsorption).

2.3. Reaction rates

Rate constants (k) at three different temperatures (60 K, 470 K, and 600 K) for each individual reaction step have been estimated from the transition state theory [79] as follows:

$$k = \left(\frac{k_B T}{h}\right)\left(\frac{q^{\neq}}{q}\right)e^{\frac{-E_a}{k_B T}} \quad (3)$$

where k_B is the Boltzmann constant, T is the absolute temperature, h is the Planck constant, and E_a the activation energy from the ZPVE corrected calculated energy barrier. Finally, $q^{\neq}$ and q are the partition functions for the TS and initial state, respectively, which have been approximated from the harmonic vibrational frequencies. The consideration of three different temperatures here is to allow comparison with different reaction mechanisms suggested from experiments working at different temperature.

3. Results

3.1. Reaction paths

Based on previous suggestions about the presence of intermediates such as NCO [42–44], N_2O [38], or $(NO)_2$ pairs [42–44] on the catalyst surfaces used in reduction of NO by CO, we propose the individual reactions shown in Scheme 1 for the global reaction.

The reaction steps included in this scheme were considered for the construction of an energy diagram of the full reduction reaction on a gold catalyst modeled here using the Au(3 2 1) surface. This requires the calculation of the adsorption energies of all the species included in Scheme 1 (reactants, intermediates, and products) and location of the transition state structures with concomitant calculation of the corresponding energies. A complete view of the individual steps connecting reactants and products of reaction is shown in Figs. 2 and 3.

Other reactions involving the same reactants as in some reactions included in Scheme 1 could be thought. However, based in the review of the literature concerning the reaction of NO reduction by CO toward CO_2 and N_2, it seems that the reactions compiled in Scheme 1 cover all suggested reactions paths, including formation of experimentally detected intermediates. For the selection of the reactions 3a–q and 4a–q, we used also knowledge that we have gained from previous computational studies and, for instance, the reaction OCOH* + OH* → $CO(OH)_2$* + *, with the same reactants as reaction 4n, was not considered since the activation energy barrier for the OCOH dehydrogenation assisted by hydroxyl, reaction 4n, is ~0 eV, i.e., these species immediately react when OCOH and OH are at reacting distance on the catalyst surface considered in this work.

3.2. Structure and stability of surface species

The most stable (co-)adsorption configurations for the species involved in the reaction steps shown in Scheme 1 were determined by considering several possible initial configurations and adsorption positions (Fig. 1) on the Au(3 2 1) surface model. Views of

NO + * → NO*			1
CO + * → CO*			2
Without hydrogen		With hydrogen	
NO* + * → N* + O*	3a	NO* + H* → NOH* + *	4a
NO* + CO* → N* + CO_2↑ + *	3b	H_2* + * → H* + H*	4b
NO* + NO* → ON_2O* + *	3c	NOH* + * → N* + OH*	4c
ON_2O* + * → N_2O* + O*	3d	NOH* + H* → N* + H_2O*	4d
N* + CO* → NCO* + *	3e	NOH* + H* → NHOH* + *	4e
N* + NO* → N_2O* + *	3f	NHOH* + * → NH* + OH*	4f
N* + N* → N_2↑ + 2*	3g	NHOH* + H* → NH_2OH* + *	4g
CO* + O* → CO_2↑ + 2*	3h	NH_2OH* + * → NH_2* + OH*	4h
NO* + O* → NO_2* + *	3i	CO* + OH* → OCOH* + *	4i
NO_2* → NO_2↑ + *	3j	NH_2OH* + H* → NH_3↑ + OH* + *	4j
NCO* + N* → N_2↑ + CO* + *	3k	H_2O* + * → OH* + H*	4k
NCO* + NO* → N_2O* + CO*	3l	OH* + * → O* + H*	4l
N_2O* → N_2↑ + O*	3m	OCOH* → CO_2↑ + H*	4m
N_2O* + CO* → N_2↑ + CO_2↑ + 2*	3n	OCOH* + OH* → CO_2↑ + H_2O* + *	4n
O_2* + * → O* + O*	3o	N* + H* → NH* + *	4o
CO* + O_2* → OCOO* + *	3p	NH* + H* → NH_2* + *	4p
OCOO* → CO_2↑ + O*	3q	NH_2* + H* → NH_3* + *	4q

Scheme 1.

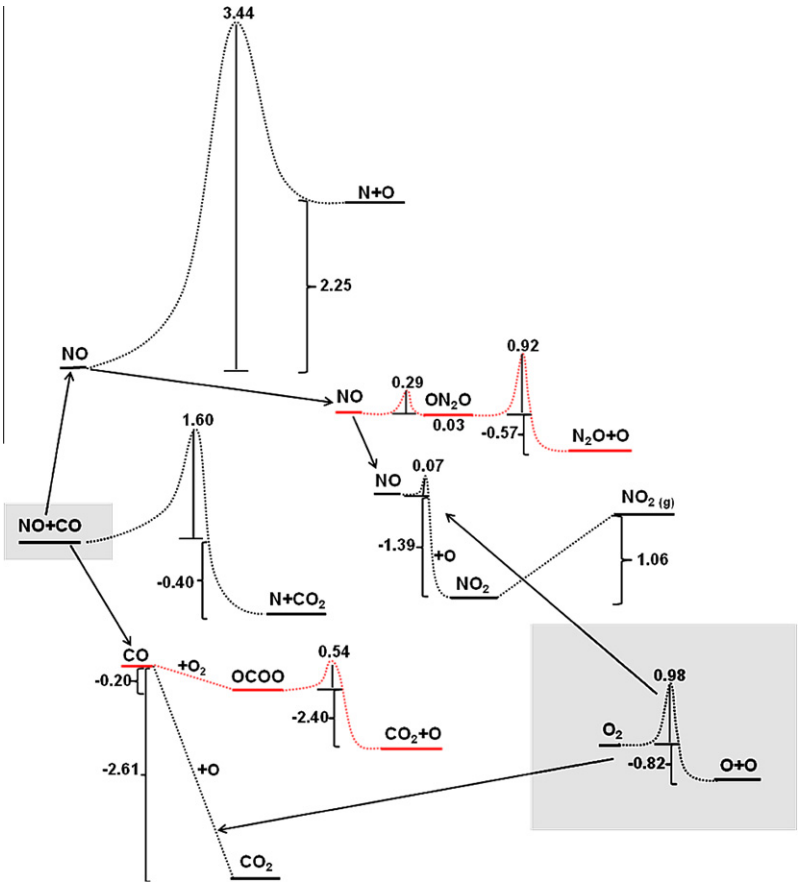

Fig. 2. Energy profiles (in eV) for NO reduction by CO in the absence of H atoms. In red are highlighted the most favorable paths. (For interpretation of the references to color in this figure legend, the reader is referred to the web version of this article.)

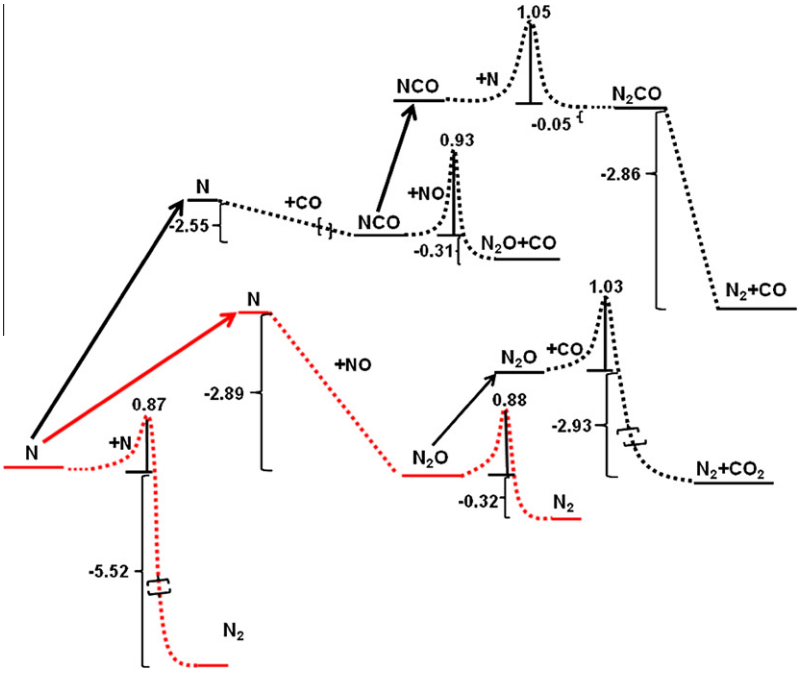

Fig. 3. Energy profiles (in eV) for reactions of N adatoms leading to gaseous nitrogen. In red are highlighted the most favorable paths. (For interpretation of the references to color in this figure legend, the reader is referred to the web version of this article.)

the most favorable configuration for each species or pair of co-adsorbed fragments can be seen in the lateral panels of Fig. S1 showed in the Supporting information (SI) and their (co-)adsorption energies are summarized in Tables 1 and 2. Extensive tables

with selected surface to adsorbate distances and internal distances for the adsorbed species are provided in Tables S1 and S2 in the Supporting information.

In the case of single species deposited onto the surface, the calculations show that the most stable adsorption sites are close to the steps of the Au(3 2 1) surface. In the cases of NO, OCOH, NH_2OH, NH_3, H_2O, and CO species, the adsorption occurs on the surface kinks while NOH, NH_2, NHOH, OH, NCO, OCOO, NO_2, ON_2O, and O_2 species interact preferentially with bridge sites at the steps. The N adatom and NH species are preferably adsorbed on the *fcc* hollow position *a*. However, even the presence of low-coordinated atoms in the model Au(3 2 1) surface seems to be not enough to stabilize strongly CO_2, N_2, H_2, and N_2O species. The preference of N, NH, and O adatoms to interact preferentially with hollow sites is kept when these species are co-adsorbed on the surface with NO, H, or CO. Furthermore, surface configurations similar to those of the isolated species are also found in the cases of pairs involving other species, *i.e.*, NO, CO, NH_2, NCO, H, O_2, H_2O, OCOH, NOH, NHOH, and OH interact preferably with kinks or bridge sites at the steps. Finally, the interactions of CO_2, N_2, and N_2O molecules with the catalyst surface are not enhanced by the presence of other species on the surface.

3.3. Reaction mechanisms

For the understanding of the mechanism of NO reduction by CO, it is necessary to locate the transition state (TS) structures and concomitant energies for the relevant elementary steps introduced in Scheme 1. Herewith, we will present separately a detailed structural and energetic description of each reaction step. Calculated data are compiled in Tables 3 and 4 for the catalytic reactions without and with the presence of hydrogen species, respectively. Extended versions of these two Tables are provided in the Supporting information, respectively, Tables S3 and S4.

The reduction of NO to N_2 on the catalyst surface requires the rupture of the N–O bond. Hence, without the presence of promoters, Fig. 2, three routes are possible, i.e., direct bond breaking ($NO^* + {}^* \rightarrow N^* + O^*$, 3a), CO assisted N-O cleavage ($NO^* + CO^* \rightarrow N^* + CO_2 + {}^*$, 3b), or disproportionation after dimerization to the ON_2O intermediate ($2NO^* \rightarrow ON_2O^* + {}^* \rightarrow N_2O^* + O^*$, 3c and 3d). The E_{act} values given in Fig. 2 are calculated as the difference between the transition state energy and those of adsorbed reactants at the most stable configuration. The calculations show that the direct NO dissociation reaction on the Au(3 2 1) model surface is not feasible since the calculated energy barrier is 3.44 eV (Table 3) and the reaction is very endothermic (2.25 eV). The reaction of N–O bond breaking assisted by CO is more favorable with a calculated energy barrier of 1.60 eV. This moderately large activation energy has to be compared with the co-adsorption energy of NO and CO on the Au(3 2 1) surface ($E_{co\text{-}ads} = -1.24$ eV) showing that this step may be possible on pure gold surfaces but only under special conditions otherwise desorption of the reactants is more favorable than the reaction mentioned above. In fact, the estimated rate constants for this reaction at different temperatures are low at 60 K and at 470 K, and at 600 K where the rate constant is $\sim 0.4\ s^{-1}\ mol^{-1}$. These results imply that the reaction can have considerable performance only at high temperatures which is compatible with the experimental observations for the reaction on gold based catalysts [52]. The reaction rate constants were estimated for temperatures of 60 K, 470 K, and 600 K, due to the fact that the $(NO)_2$ pairs are already detected at very low temperatures [45,46] and the direct reaction of NO with CO occurs only at high temperatures [52]; note also that in the experimental work of Debeila et al. the $(NO)_2$ pairs were observed at low temperature and they seem to be stable up to ~100 °C. The rupture of the N–O bond after dimerization of NO to yield the ON_2O surface species is much more favorable than any of the two reactions above. The computed energy barriers are 0.29 eV and 0.92 eV for the $2NO^* \rightarrow ON_2O^* + {}^*$ and $ON_2O^* + {}^* \rightarrow N_2O^* + O^*$ elementary steps, respectively. The calculated co-adsorption energy for the reactants

Table 1
Calculated ZPVE corrected interaction energies (in eV) for isolated species deposited on the Au(3 2 1) surface.

Species	Adsorption site	E^o_{ads}
NO	top "1"	−0.71
CO	top "1"	−0.72
N_2	far from surface	−0.03
CO_2	far from surface	−0.10
OCOO	b_{2-1}	−0.91
N_2O	far from surface	0.00
O_2	b_{1-2}	−0.15
NCO	b_{2-1}	−2.32
OH	b_{2-1}	−2.30
OCOH	top "1"	−3.52
N	hole "a"	−2.60
ON_2O	b_{1-2}–top "3"	−1.33
NOH	b_{2-1}	−2.41
NHOH	b_{2-1}	−1.12
H_2O	top "1"–step	−0.23
H_2	far from surface	−0.06
NO_2	b_{2-1}	−0.98
NH_2OH	top "1"–step	−0.69
NH	hole "a"	−2.50
NH_2	b_{2-1}	−2.00
NH_3	top "1"	−0.53

Table 2
Calculated ZPVE corrected interaction energies (in eV) for pairs deposited on the Au(321) surface.

Species	Co-adsorption sites	E^o_{co-ads}
NO + CO	top "2"–top "1"	−1.18
N + N	hole "d"– hole "h"	−4.99
NO + NO	top "1"–top "3"	−1.37
N_2O + O	far from surface–hole "a"	−3.30
N + NO	hole "a"– b_{2-1}	−3.16
N_2 + O	far from surface–hole "a"	−3.24
N_2O + CO	far from surface–b_{2-1}	−0.60
N_2 + CO_2	far from surface–far from surface	−0.11
N + CO_2	hole "a"– far from surface	−2.60
N + OH	hole "b"–b_{3-1}	−4.97
N + O	hole "d"–hole "h"	−5.82
NH + OH	hole "b"–b_{3-1}	−4.83
NO + H	top "1"–hole "d"	−2.53
NOH + H	b_{2-1}–b_{4-1}	−4.23
N + H_2O	hole "a"–step	−2.92
NCO + NO	top "1"–top "2"	−2.82
NCO + N	top "1"–hole "a"	−4.83
N_2 + CO	far from surface–top "1"	−0.76
O + H	hole "a"–b_{4-1}	−5.53
CO + OH	top "1"–top "2"	−2.83
CO_2 + H	far from surface–b_{2-1}	−2.16
OCOH + OH	top "1"–b_{3-1}	−3.40
CO_2 + H_2O	far from surface–step	−0.42
O + O	hole "d"–hole "h"	−6.50
CO + O	top "1"–hole "d"	−0.66
CO + O_2	top "1"–top "2"	−0.71
CO_2 + O	far from surface–hole "a"	−0.13
N + CO	hole "h"–top "1"	−3.20
OH + H	b_{1-2}–b_{4-1}	−4.24
H + H	b_{1-2}–b_{2-1}	−3.74
NO + O	top "1"–hole "a"	−3.84
NHOH + H	b_{2-1}–b_{1-2}	−4.04
NH_2 + OH	top "1"–b_{2-3}	−3.57
NH_2OH + H	top "1"–b_{1-2}	−2.58
NH_3 + OH	far from surface–b_{1-2}	−2.31
N + H	hole "a"–b_{4-1}	−4.84
NH + H	hole "a"–b_{4-1}	−4.72
NH_2 + H	b_{1-2}–b_{4-1}	−3.96

Table 3
Calculated data for the different elementary steps considered in the reaction of NO reduction by CO in the absence of hydrogen.[a]

Elementary step	TSBL	E^{o}_{act}	Δ_o	k			ν
				60 K	470 K	600 K	
$NO^* \rightarrow N^* + O^*$	2.12	3.44	2.25	2.7×10^{-267}	1.7×10^{-23}	1.1×10^{-15}	348*i*
$NO^* + CO^* \rightarrow N^* + CO_2{}^{\uparrow}$	1.83	1.60	−0.40	7.6×10^{-123}	5.5×10^{-5}	3.6×10^{-1}	476*i*
$NO^* + NO^* \rightarrow ON_2O^*$	1.87	0.29	0.03	7.8×10^{-14}	$7.8 \times 10^{+8}$	$4.6 \times 10^{+9}$	167*i*
$ON_2O^* \rightarrow N_2O^* + O^*$	1.74	0.92	−0.57	1.9×10^{-66}	$5.4 \times 10^{+2}$	$9.5 \times 10^{+4}$	463*i*
$N^* + CO^* \rightarrow NCO^*$	–	0.00	−2.55	–	–	–	–
$N^* + NO^* \rightarrow N_2O^*$	–	0.00	−2.89	–	–	–	–
$N^* + N^* \rightarrow N_2{}^{\uparrow}$	2.18	0.87	−5.52	7.5×10^{-62}	$4.4 \times 10^{+3}$	$6.0 \times 10^{+5}$	410*i*
$CO^* + O^* \rightarrow CO_2{}^{\uparrow}$	–	0.00	−2.61	–	–	–	–
$NO^* + O^* \rightarrow NO_2{}^* + {}^*$	2.50	0.07	−1.39	$5.5 \times 10^{+6}$	$4.2 \times 10^{+12}$	$7.7 \times 10^{+12}$	120*i*
$NO_2{}^* \rightarrow NO_2 + {}^*$	–	1.06	1.06	3.6×10^{-77}	$2.2 \times 10^{+2}$	$8.4 \times 10^{+4}$	–
$NCO^* + N^* \rightarrow N_2{}^* + CO^*$	2.01	1.05	−2.91	3.5×10^{-77}	$3.1 \times 10^{+1}$	$1.1 \times 10^{+4}$	218*i*
$NCO^* + NO^* \rightarrow N_2O^* + CO^*$	1.85	0.93	−0.31	3.5×10^{-67}	$7.6 \times 10^{+2}$	$1.4 \times 10^{+5}$	295*i*
$N_2O^* \rightarrow N_2{}^{\uparrow} + O^*$	1.54	0.88	−0.32	6.3×10^{-63}	$1.1 \times 10^{+3}$	$1.6 \times 10^{+5}$	480*i*
$N_2O^* + CO^* \rightarrow N_2{}^{\uparrow} + CO_2{}^{\uparrow}$	1.51	1.03	−2.93	6.7×10^{-76}	$3.5 \times 10^{+1}$	$1.1 \times 10^{+4}$	545*i*
$O_2{}^* \rightarrow O^* + O^*$	1.91	0.98	−0.82	4.2×10^{-71}	$1.8 \times 10^{+2}$	$4.3 \times 10^{+4}$	620*i*
$CO^* + O_2{}^* \rightarrow OCOO^*$	–	0.00	−0.20	–	–	–	–
$OCOO^* \rightarrow CO_2{}^{\uparrow} + O^*$	1.77	0.54	−2.40	6.4×10^{-34}	$1.2 \times 10^{+7}$	$2.8 \times 10^{+8}$	842*i*

[a] Length of the breaking or forming bond in the TS (TSBL, Å); activation energy (E^{o}_{act}, eV); reaction energy (Δ_o, eV); reaction rate constants (k, s^{-1}, or $mol^{-1}\ s^{-1}$); imaginary frequency in the TS (ν, cm^{-1}).

Table 4
Calculated data for the different elementary steps considered in the reaction of NO reduction by CO in the presence of hydrogen.[a]

Elementary step	TSBL	E^{o}_{act}	Δ_o	k			ν
				60 K	470 K	600 K	
$H_2{}^* + {}^* \rightarrow H^* + H^*$	1.33	0.52	0.29	3.8×10^{-32}	$2.1 \times 10^{+7}$	$4.3 \times 10^{+8}$	928*i*
$NO^* + H^* \rightarrow NOH^*$	1.28	0.54	0.28	7.8×10^{-34}	$1.3 \times 10^{+7}$	$3.0 \times 10^{+8}$	824*i*
$NOH^* \rightarrow N^* + OH^*$	2.07	1.28	0.10	7.1×10^{-96}	1.7×10^{-1}	$2.0 \times 10^{+2}$	206*i*
$NOH^* + H^* \rightarrow N^* + H_2O^*$	1.47	0.44	−1.13	1.2×10^{-25}	$1.4 \times 10^{+8}$	$1.8 \times 10^{+9}$	648*i*
$NOH^* + H^* \rightarrow NHOH^*$	1.79	0.24	−1.47	1.7×10^{-08}	$3.0 \times 10^{+10}$	$1.4 \times 10^{+11}$	467*i*
$NHOH^* \rightarrow NH^* + OH^*$	2.25	1.22	−0.06	1.9×10^{-91}	5.2×10^{-2}	$4.5 \times 10^{+2}$	163*i*
$H_2O^* \rightarrow OH^* + H^*$	1.86	1.33	1.19	1.7×10^{-100}	3.5×10^{-2}	$5.4 \times 10^{+1}$	398*i*
$CO^* + OH^* \rightarrow OCOH^*$	–	0.00	−0.69	–	–	–	–
$OCOH^* \rightarrow CO_2 + H^*$	1.44	0.71	−0.36	6.3×10^{-49}	$4.4 \times 10^{+4}$	$2.5 \times 10^{+6}$	876*i*
$OCOH^* + OH^* \rightarrow CO_2{}^{\uparrow} + H_2O^*$	–	0.00	−1.96	–	–	–	–
$OH^* \rightarrow O^* + H^*$	1.69	1.82	1.31	2.6×10^{-141}	2.8×10^{-7}	6.0×10^{-3}	512*i*
$NHOH^* + H^* \rightarrow NH_2OH^*$	2.05	0.22	−1.30	7.8×10^{-7}	$5.0 \times 10^{+10}$	$2.0 \times 10^{+11}$	324*i*
$NH_2OH^* \rightarrow NH_2{}^* + OH^*$	1.93	0.82	0.18	2.3×10^{-57}	$1.1 \times 10^{+4}$	$1.1 \times 10^{+6}$	253*i*
$NH_2OH^* + H^* \rightarrow NH_3{}^* + OH^*$	1.78	0.20	−1.37	6.7×10^{-6}	$2.6 \times 10^{+10}$	$9.5 \times 10^{+10}$	345*i*
$N^* + H^* \rightarrow NH^*$	1.66	0.62	−1.32	8.5×10^{-41}	$2.1 \times 10^{+6}$	$7.6 \times 10^{+7}$	819*i*
$NH^* + H^* \rightarrow NH_2{}^*$	1.73	0.57	−1.33	2.0×10^{-36}	$7.8 \times 10^{+6}$	$2.1 \times 10^{+8}$	619*i*
$NH_2{}^* + H^* \rightarrow NH_3{}^*$	1.82	0.71	−1.19	2.2×10^{-48}	$2.3 \times 10^{+5}$	$1.3 \times 10^{+7}$	454*i*

[a] Length of the breaking or forming bond in the TS (TSBL, Å); activation energy (E^{o}_{act}, eV); reaction energy (Δ_o, eV); reaction rate constants (k, s^{-1}, or $mol^{-1}\ s^{-1}$); imaginary frequency in the TS (ν, cm^{-1}).

is −1.37 eV and the reaction energies are 0.03 eV and −0.57 eV, respectively. The rate constants calculated for these two reactions suggest that these can occur at moderate temperatures. Furthermore, the relative easy formation of ON_2O^* based on its calculated activation energy barrier of only 0.29 eV is in perfect agreement with the observation of $(NO)_2$ pairs at low temperatures on gold based catalysts [45,46].

Nitrogen adatoms will be formed in the case of the CO aided N-O cleavage, which can react with additional CO or NO species, Fig. 3, leading to NCO or N_2O, respectively. The latter species is also formed in the reaction of disproportionation via ON_2O^*. The calculations show that either NCO or N_2O are easily formed on the surface – ZPVE corrected activation energies for the reactions $N^* + CO^* \rightarrow NCO^* + {}^*$ (3e) and $N^* + NO^* \rightarrow N_2O^* + {}^*$ (3f) are zero – and therefore one can expect that these reactions are controlled by diffusion of the surface species or that N^* reacts directly with gaseous NO or CO (Eley–Rideal mechanism). The estimated energy barriers for diffusion of the reacting species from their most favorable adsorption sites to the sites they occupy before reaction on the surface steps are 0.3 eV for N^* and 0.1 eV for CO^* and for NO^*. These values were obtained by taking 12% of their adsorption energies [68,80]; in the case of O adatom, estimated ($0.12 \times 3.21 = 0.39$ eV) and calculated (0.42 eV) ZPVE corrected diffusion barriers differ by only 0.03 eV. Nitrogen adatoms may also combine on the surface to form molecular nitrogen (Fig. 3). The calculated energy barrier for the $N^* + N^* \rightarrow N_2 + 2^*$ (3g) reaction is 0.87 eV and dramatically exothermic (−5.52 eV, Table 3).

As can be seen in Fig. 2, oxygen adatoms formed on the surface via disproportionation after dimerization can further react with additional CO or NO species yielding CO_2 ($CO^* + O^* \rightarrow CO_2 + 2^*$, 3h) or NO_2 ($NO^* + O^* \rightarrow NO_2{}^* + {}^*$, 3i), respectively. These two oxidation reactions were already been treated in separate works. They proceed with small activation energy barriers on the Au(3 2 1) surface, 0.00 eV in the case of CO oxidation [69] and 0.07 eV in the case of NO oxidation [81], and CO_2 is easily desorbed from the surface while NO_2 is strongly adsorbed on the surface and requires 1.06 eV to be released from the catalyst ($NO_2{}^* \rightarrow NO_2 + {}^*$, 3j) [69,81].

Molecular nitrogen and carbon dioxide may be obtained from the NCO intermediate directly via $NCO^* + N^* \rightarrow N_2CO^* + {}^* \rightarrow N_2 + CO^* + {}^*$ (3k) followed by $CO^* + O^* \rightarrow CO_2 + 2^*$ (3h). The calculated barrier for the former reaction is 1.05 eV, which is exothermic

by 2.91 eV (Fig. 3). The NCO intermediate can react with NO* species to yield the N_2O intermediate, c.f. $NCO^* + NO^* \rightarrow N_2O^* + CO^*$ (3l), with a concomitant barrier of 0.93 eV. From the N_2O intermediate it is possible to obtain molecular nitrogen ($N_2O^* \rightarrow N_2 + O^*$, 3m; energy barrier is 0.88 eV) or directly the desired reaction products ($N_2O^* + CO^* \rightarrow N_2 + CO_2 + 2^*$, 3n, energy barrier is 1.03 eV). Interestingly, these reactions have moderately high activation energies which are close to that calculated for dissociation of molecular oxygen ($O_2^* \rightarrow O^* + O^*$, 3o, 0.98 eV). Finally, the CO* species can also react with molecular oxygen adsorbed on the catalytic surface yielding, without energy barrier, the OCOO surface species ($CO^* + O_2^* \rightarrow OCOO^* + ^*$, 3p), which was proposed in an experimental work as an intermediary in the CO oxidation by molecular oxygen when the reaction is catalyzed by gold atoms [82]. The OCOO species latter can further decompose to yield carbon dioxide ($OCOO^* \rightarrow CO_2 + O^*$, 3q) with associated activation and reaction energies of 0.54 eV and −2.40 eV, respectively.

Previous experimental studies suggest for some gold-supported catalysts that hydrogen is crucial for NO reduction at temperatures between 473 K and 623 K and that it acts as a promoter of the reaction [42,56]. However, its role is not well understood since at temperatures higher than 623 K the presence of hydrogen seems to have an opposite effect [42,56]. Probably, hydrogen species are needed for the formation of partly charged active gold particles. The results of DFT calculations on some possible reaction paths (Scheme 1) involving hydrogen on the NO + CO reaction will be reported below. As found above, the direct dissociation of NO producing N and O adatoms has to surmount a prohibitive activation barrier and, if hydrogen species act as promoters they will combine with NO* species before N–O bond cleavage (Fig. 4). The most favorable reaction is that producing NOH* ($NO^* + H^* \rightarrow NOH^* + ^*$, 4a), which requires previous dissociation of molecular hydrogen ($H_2^* + ^* \rightarrow H^* + H^*$, 4b) [56]. These reactions are slightly endothermic and their energy barriers are 0.54 eV and 0.52 eV, respectively.

From the NOH* intermediate, three different reaction paths are possible [56], *i.e.*, direct N-O cleavage ($NOH^* + ^* \rightarrow N^* + OH^*$, 4c), H*-aided N–O rupture ($NOH^* + H^* \rightarrow N^* + H_2O^*$, 4d), and N–O bond break after formation of another hydrogenated species ($NOH^* + H^* \rightarrow NHOH^* + ^* \rightarrow NH^* + OH^*$, 4e and 4f). The most favorable reaction path is 4d with an energy barrier of 0.44 eV and reaction energy of −1.13 eV. The reactions 4c and 4f have barriers of 1.28 eV and 1.22 eV, respectively. From this point, N* adatoms will diffuse on the surface and eventually molecular nitrogen will desorb from the catalyst surface as shown above via reaction 3 g. Importantly, reaction 4d has to compete with the reaction producing the hydroxylimine species (NHOH, 4e) which has a barrier of only 0.24 eV. Dissociation of NHOH* (4f) is, however, rather difficult since the energy required for the N–O bond break (1.22 eV) is larger than its adsorption energy (−1.12 eV), and, hence, it is expected to occur under special conditions. Therefore, one can anticipate that a series of stepwise addition reactions will take place and eventually they will lead to the formation of ammonia. In fact, hydroxylimine will react easily (calculated energy barrier of only 0.22 eV) with additional hydrogen adatoms to produce hydroxylamine ($NHOH^* + H^* \rightarrow NH_2OH^* + ^*$, 4 g). Hydroxylamine can further react with additional H* adatoms or it can suffer N–O bond cleavage. The dissociation of the N–O bond in NH_2OH^* ($NH_2OH^* + ^* \rightarrow NH_2^* + OH^*$, 4 h) has an energy barrier of 0.82 eV. The adsorption energy calculated for NH_2OH^* is −0.78 eV and therefore, within the uncertainties associated with the computational approach, the cleavage of the N–O bond in hydroxylamine is suggested to occur, eventually leading to the formation of OH* radicals that can react with CO* (4i). The latter reaction is in competition with

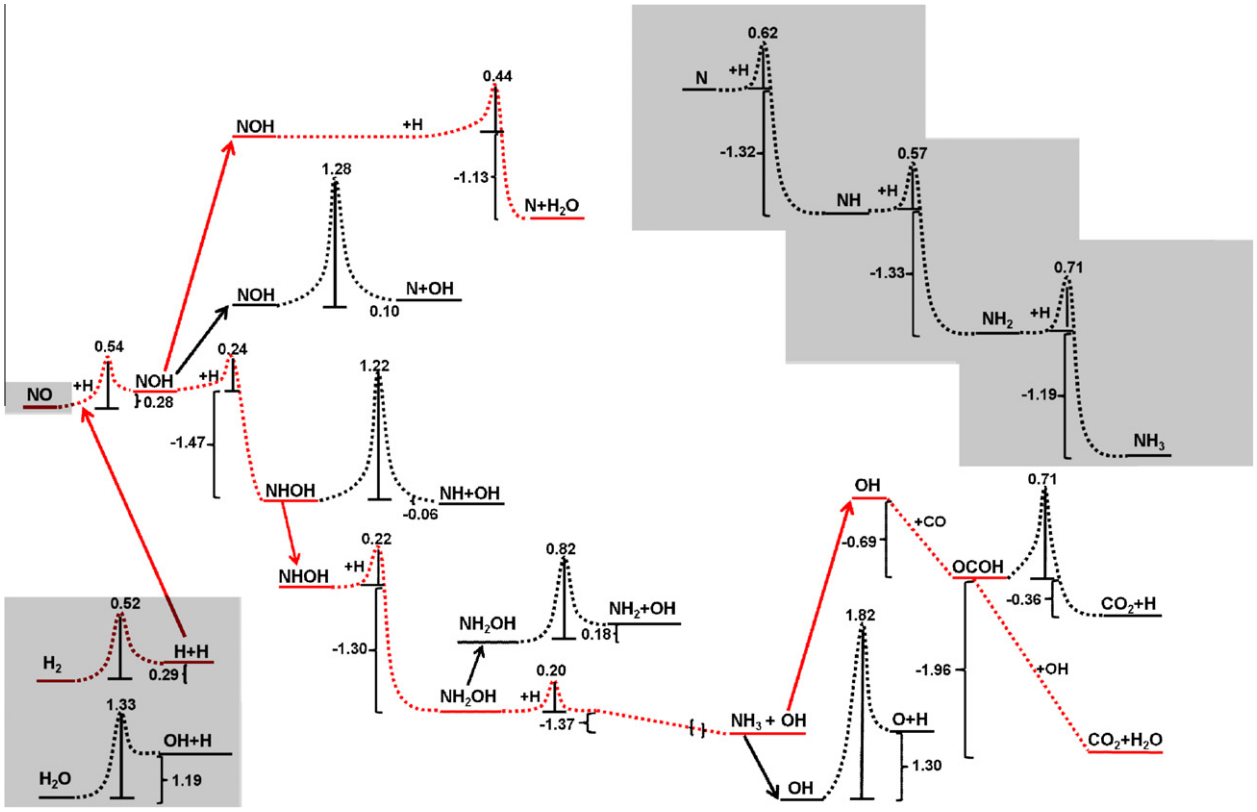

Fig. 4. Energy profiles (in eV) for NO reduction by CO in presence of H atoms. In red are highlighted the most favorable paths. (For interpretation of the references to color in this figure legend, the reader is referred to the web version of this article.)

that where NH_2OH^* reacts with additional hydrogen adatoms, i.e., $NH_2OH^* + H^* \rightarrow NH_3OH^* + *$. We could not find any transition state structure leading to the formation of surface NH_3OH species. The dimer calculations yielded a TS, where the products of the reaction between NH_2OH^* and H^* yielded a surface OH^* radical and a NH_3 species at a significant distance from the catalyst model surface suggesting that the reaction will lead to the formation of gaseous ammonia, i.e., $NH_2OH^* + H^* \rightarrow NH_3^{\uparrow} + OH^* + *$, 4j. This reaction step was calculated to be highly exothermic (−1.37 eV) and it has an associated energy barrier of only 0.20 eV. The energy barriers for the different reactions based on the NOH intermediate show that hydrogen has an important effect on the reaction of NO reduction catalyzed by gold as found experimentally [57]. However, the reaction of N–O bond dissociation aided by H^* species is in competition with the stepwise reactions leading to the production of gaseous NH_3 and surface OH^* species. Based on experimental findings, it seems that the latter reaction gains importance at temperatures larger than ~500 K [57]. Since the calculated activation energy barriers for reactions 4e, 4g, and 4j are smaller than the barrier computed for reaction 4d, the experimental results can be explained on the basis of lower probability of subsequent addition of H^* adatoms to the nitrogen of the NH_xOH species in the case of the stepwise reactions when compared with the probability of addition of H^* adatom to the oxygen of NOH species in the case of reaction 4d.

Based on previous computational studies, the fate of the NH and NH_2 species, if formed, seems to be reaction with surface O^* species with concomitant activation energy barriers lower than 0.9 eV [83], since the reactions toward ammonia ($NH_x^* + H^*$) have to surpass barriers larger than 1.1 eV on the very reactive Ru surfaces [84] and the reactions of dehydrogenation ($NH_x^* - H^*$) to N^* and H^* adatoms have to surpass barriers larger than 2.7 eV on Au(1 1 1) [83], conferring to the Ru based catalysts a high selectivity toward N_2 and NH_3 production will be a minor step [85]. Catalysts based on ruthenium were found in fact to be highly selective toward N_2 in the catalytic reduction of NO when compared with other transition metals, where larger proportions of NH_3 were formed [85–87]. In the case of gold, the direct route leading to NH_3 production, i.e., successive addition of H atoms to N, is also possible. This route, reactions 4o, 4p, and 4q, was also studied in this work considering the Au(3 2 1) surface as a gold catalyst model. The activation energy barrier for the NH^* formation reaction ($N^* + H^* \rightarrow NH$, 4o) presents a value of 0.62 eV, which is higher than the activation energy barriers obtained for the route via the NH_xOH species described above. Furthermore, the activation energies for the subsequent hydrogenation reactions, $NH^* + H^* \rightarrow NH_2^* + *$, 4p, and $NH_2^* + H^* \rightarrow NH_3^* + *$, 4q, are 0.57 eV and 0.71 eV, respectively. These values suggest that the route proposed above via the NH_xOH species is clearly more favorable than the direct route for the NH_3 production. Nevertheless, evolution through the direct route cannot be discarded due to the moderate activation energy barriers calculated for reactions 4o, 4p, and 4q. From what was written above, gold based catalysts are predicted to be unselective toward N_2 production and NH_3 will be also formed as described in the next sub-section.

In the experimental works of Ilieva et al., it is observed that water vapor in the gas feed ($NO + CO + H_2 + H_2O$) increases the activity of gold-supported catalysts to N_2 working at temperatures below ~500 K [57,58]. These authors suggest that the water gas shift reaction will add additional amounts of hydrogen that promote the NO reduction by CO [57,58]. Our calculations suggest that in the case of pure gold catalysts, the experimentally suggested formation of hydrogen via the reaction of water dissociation ($H_2O^* + * \rightarrow H^* + OH^*$, 4k, and $OH^* + * \rightarrow H^* + O^*$, 4l) is challenging due to the moderately high energy barriers calculated for these reactions, *i.e.*, barriers of 1.33 eV [88] and 1.82 eV, respectively. Thus, the support seems to have an important role in catalyzing the reaction of water dissociation which is in agreement with very recent findings, where the metal–oxide interface in the case of gold nanoparticles deposited on titania was found to have an essential role in the catalysis of the water splitting reaction [89].

The OH species formed in the reactions above (reactions 4c, 4k, 4f, 4h, and, more probably, reaction 4j) can further react with CO^* and be the source of the carboxyl intermediate ($OCOH^*$) since the $CO^* + OH^* \rightarrow OCOH^* + *$ (4i) reaction is barrierless. This compound will eventually decompose directly ($OCOH^* \rightarrow CO_2 + H^*$, 4m) or OH^*-assisted ($OCOH^* + OH^* \rightarrow CO_2 + H_2O^* + *$, 4n) to gaseous carbon dioxide. The former has to proceed through an energetic barrier of 0.71 eV (Table 4) while the latter reaction is barrierless.

3.4. Most favorable routes

From the extensive analysis of several potential reaction pathways for the reduction of NO by CO, it is now possible to suggest the most favorable cases in the absence and in the presence of hydrogen species. If hydrogen species are not available on the catalytic gold surface, the most favorable mechanism leading to the formation of N_2 and CO_2 gaseous molecules is via the following reaction steps:

$$2NO^* \rightarrow ON_2O^* + *(E_{act} = 0.29\ eV);$$
$$ON_2O^* + * \rightarrow N_2O^* + O^*(E_{act} = 0.92\ eV);$$
$$N_2O^* \rightarrow N_2 + O^*(E_{act} = 0.88\ eV);$$
$$CO^* + O^* \rightarrow CO_2 + 2^*(E_{act} = 0.00\ eV),$$

i.e., where $(NO)_2$ pairs are formed initially at low temperature and with the increase of temperature the reaction proceeds to the evolution of gaseous N_2 and CO_2 from the catalyst surface, which is in excellent agreement with the experimental observations [52].

In the presence of hydrogen species, the most favorable reaction mechanism leading to N_2 and CO_2 is that via the reactions below:

$$H_2 + 2^* \rightarrow H^* + H^*(E_{act} = 0.52\ eV);$$
$$NO^* + H^* \rightarrow NOH^* + *(E_{act} = 0.54\ eV);$$
$$NOH^* + H^* \rightarrow N^* + H_2O^*(E_{act} = 0.44\ eV);$$
$$N^* + NO^* \rightarrow N_2O^* + *(E_{act} = 0.00\ eV);$$
$$N_2O^* \rightarrow N_2 + O^*(E_{act} = 0.88\ eV);$$
$$CO^* + O^* \rightarrow CO_2 + 2^*(E_{act} = 0.00\ eV),$$

for which the largest energy barrier is 0.88 eV, i.e., 0.04 eV lower than that calculated for the reaction without the hydrogen species onto the catalyst. In the mechanism above, the following reaction step

$$N^* + N^* \rightarrow N_2 + 2^*(E_{act} = 0.87\ eV);$$

is also possible and competes with the reaction forming O^* adatoms from N_2O^*.

However, if hydrogen species are available, the former mechanism has to compete with the reaction leading to formation of NH_3, H_2O, and CO_2 as shown in the reactions below:

$$H_2 + 2^* \rightarrow H^* + H^*(E_{act} = 0.52\ eV);$$
$$NO^* + H^* \rightarrow NOH^* + *(E_{act} = 0.54\ eV);$$
$$NOH^* + H^* \rightarrow NHOH^* + *(E_{act} = 0.24\ eV);$$
$$NHOH^* + H^* \rightarrow NH_2OH^* + *(E_{act} = 0.22\ eV);$$
$$NH_2OH^* + H^* \rightarrow NH_3 + OH^* + *(E_{act} = 0.20\ eV);$$
$$CO^* + OH^* \rightarrow OCOH^* + *(E_{act} = 0.00\ eV);$$
$$OCOH^* + OH^* \rightarrow CO_2 + H_2O^* + *(E_{act} = 0.00\ eV),$$

where the largest energy barrier is only 0.54 eV, *i.e.*, approximately 40% smaller than the activation energies for the other two reaction mechanisms above. Formation of N_2 and NH_3 was reported

experimentally for gold-supported catalysts [90]. These results agree with the observation of traces of N_2O^* species when hydrogen species are available to react with NO [91,92], i.e., this mechanism via NOH^* and NH_xOH^* intermediates is more favorable than that through NOH^* and N_2O^*. The combination of the information coming from the latter energy barriers with the fact that activation energies for the hydrogenation of NH_x species are larger than 1.1 eV, even on the very reactive Ru surfaces [84], suggests that the formation of ammonia observed experimentally on Pt–Rh alloy catalysts [92] proceeds through NH_xOH^* instead of via NH_x^* species. In fact, the experimental band in the HREELS spectrum found at 3200 cm^{-1} [92] and attributed to NH_x^* interacting with a Pt–Rh alloy catalyst does not exclude the formation of NOH^* and NH_xOH^* for which frequencies in the range 3350–3600 cm^{-1} were calculated, cf. Table S5 in the supporting information.

The experimental observation of the NCO species adsorbed on Au phase at moderate temperatures [42–44] – Fourier transform infrared spectroscopy (FTIR) bands in the range 2185–2195 cm^{-1} as determined on several Au/metal oxide catalysts agree well with the calculated value for the N–C stretching on Au(3 2 1) that is 2239.5 cm^{-1} – suggests direct reaction of some NO and CO molecules (reaction 3b) but the results from our calculations indicate that this reaction will be rather improbable (E_{act} = 1.60 eV) on clean gold surfaces. Nevertheless, the presence of small amounts of hydrogen species onto the surface will facilitate the formation of this intermediate since if nitrogen adatoms are formed during the reduction reactions, for instance via reaction 4d, they can readily react with available carbon monoxide molecules to yield, without energy barrier, surface isocyanate species.

Finally, the estimated rate constants show that several of the reactions considered in this work are not easy even at 600 K.

3.5. Final remarks

The formation of ammonia during the catalytic NO removal from the automobile exhaust is well documented as the principal problem in the design of catalysts for controlling exhaust gases [86]. Ruthenium based catalysts were found to be highly selective for N_2 formation due to the high activation energy barriers calculated for the NH_3 formation [84]. Other metal based catalysts were found experimentally to be less selective [85,87]. In the work of Klimisch and Taylor, it is reported that copper catalysts (or platinum) reduce nitric oxide to ammonia and that nickel is ineffective for nitric oxide reduction but it is able to decompose ammonia. In the case of gold, this metal was considered to be quite inert for hydrogenation reactions but surprisingly it was found in the past to be active for the reduction of NO by H_2 leading either to N_2 or to NH_3 [90]. In fact, and quite interestingly, the oxide support used to deposit the gold catalyst was found to have a role in the selectivity of the catalyst toward N_2 formation.

It is quite encouraging to find that the results from this computational work are in agreement with the available experimental data listed above. Furthermore, based on the calculated energy barriers on the Au(3 2 1) model surface, this computational study gives support to the possible formation of some intermediates that were suggested in previous experimental work [54], which can be formed at the conditions used in those experimental works.

4. Conclusions

Periodic density functional theory calculations have been used to explore several different reaction routes connecting the gaseous molecules NO and CO as reactants and N_2 and CO_2 as products catalyzed by a Au(321) model surface. The calculations suggest as the most feasible reaction paths for the $NO + CO \rightarrow ½\ N_2 + CO_2$ global reaction the route $2NO + 2CO \rightarrow ON_2O + 2CO \rightarrow N_2O + O + 2CO \rightarrow N_2 + 2O + 2CO \rightarrow N_2 + 2CO_2$ in the absence of hydrogen species on the catalyst surface, i.e., via the ON_2O and N_2O intermediates, and the route $2NO + CO + H_2 \rightarrow 2NO + CO + 2H \rightarrow NO + NOH + CO + H \rightarrow NO + N + CO + H_2O \rightarrow N_2O \rightarrow CO + H_2O \rightarrow N_2 + O + CO + H_2O \rightarrow N_2 + CO_2 + H_2O$ if hydrogen species are present on the catalyst surface, i.e., via NOH and N_2O intermediates. Interestingly, the two routes above have to surpass activation energy barriers of up to ~0.9 eV. However, the calculations predicted a much more favorable reaction path (maximum energy barrier of 0.54 eV) when hydrogen is present at the catalyst surface, where ammonia and not molecular nitrogen is the nitrogenated product of the reaction. The complete path is $2NO + CO + 4H_2 \rightarrow 2NO + CO + 8H \rightarrow 2NOH + CO + 6H \rightarrow 2NHOH + CO + 4H \rightarrow 2NH_2OH + CO + 2H \rightarrow 2NH_3 + 2OH + CO \rightarrow 2NH_3 + OH + OCOH \rightarrow 2NH_3 + CO_2 + H_2O$.

For comparison purposes, the reaction of CO with molecular oxygen, i.e., $CO + O_2 \rightarrow OCOO \rightarrow CO_2 + O$ has the same activation energy. These routes are calculated to be clearly exothermic.

The calculations show that NCO, an intermediate that was suggested to be present in the course of the NO reduction reaction by CO, is easily formed if nitrogen adatoms are available on the catalyst surface. In fact, N adatoms reaction with CO proceeds without energy barrier. The isocyanate intermediate can yield N_2O and CO, energy barrier of 0.93 eV, or at higher temperatures it can evolute toward N_2 and CO molecules by surmounting a energy barrier of 1.05 eV. Nevertheless, since these barriers are higher than those for the most favorable reaction mechanisms either in the presence or absence of surface hydrogen species, these species are suggested to be just spectators at moderate temperatures.

Finally, almost all the surface species considered in this work are adsorbed preferentially at regions nearby the steps of the Au(3 2 1) model surface, which is a clear sign of the importance that low-coordinated atoms can have in the course of catalytic reactions.

Acknowledgments

Thanks are due to Fundação para a Ciência e Tecnologia (FCT), Lisbon, Portugal, Programme Ciência 2007, and to FEDER for financial support to REQUIMTE and to CICECO (Pest-C/EQB/LA0006/2011 and Pest-C/CTM/LA0011/2011). JLCF acknowledges FCT for the Grant SFRH/BPD/64566/2009 co-financed by the Fundo Social Europeu (FSE).

Appendix A. Supplementary material

Supplementary data associated with this article can be found, in the online version, at doi:10.1016/j.jcat.2012.01.010.

References

[1] Proposal for a Regulation of the European Parliament and of the council; on type approval of motor vehicles with respect to emissions and on access to vehicle repair information, amending Directive 72/306/EEC and Directive ../../EC (presented by the Commission). {SEC(2005) 1745}, 2005/0282 (COD), COM(2005), 683 final, 21.12.2005, Brussels, 2005.
[2] Inventory of US Greenhouse Gas Emissions and Sinks: 1990–2008, April 15, <http://epa.gov/climatechange/emissions/usinventoryreport.html>, 2010 (accessed 20.10.10).
[3] C.D. Chang, J.G. Santiesteban, D.S. Shihabi, S.A. Stevenson, US Patent 5 401 478 (1995), to Mobil Oil Corporation.
[4] N. Miyoshi, S. Matsumoto, K. Katoh, T. Tanaka, J. Harada, N. Takahashi, K. Yokota, M. Suguira, K. Kasahara, SAE Technical Paper 950809, 1995.
[5] S. Matsumoto, Y. Ikeda, H. Suzuki, M. Ogai, N. Miyoshi, Appl. Catal. B: Environ. 25 (2000) 115.
[6] F. Garin, Appl. Catal. A: Gen. 222 (2001) 183.
[7] R. Meyer, C. Lemire, S.K. Shaikhutdinov, H.-J. Freund, Gold Bull. 37 (2004) 72.
[8] L.D. Li, J.J. Yu, Z.P. Hao, Z.P. Xu, J. Phys. Chem. C 111 (2007) 10552.

[9] P.S. Lambrou, P.G. Savva, J.L.G. Fierro, A.M. Efstathiou, Appl. Catal. B: Environ. 76 (2007) 375.
[10] M. Haneda, Pusparatu, Y. Kintaichi, I. Nakamura, M. Sasaki, T. Fujitani, H. Hamada, J. Catal. 229 (2005) 197.
[11] S. Zhu, X. Wang, A. Wang, T. Zhang, Catal. Today 131 (2008) 339.
[12] R. Zhu, M. Guo, X. Ci, F. Ouyang, Catal. Commun. 9 (2008) 1184.
[13] M. Marwood, C.G. Vayenas, J. Catal. 170 (1997) 275.
[14] J.C. Chen, F.Y. Chang, M.Y. Wey, Catal. Commun. 9 (2008) 1106.
[15] A. de Oliveira, I.M. Baibich, N.R.C.F. Machado, M.L. Mignoni, S.B.C. Pergher, Catal. Today 133 (2008) 560.
[16] S. Hammache, L.R. Evans, E.N. Coker, J.E. Miller, Appl. Catal. B: Environ. 78 (2008) 315.
[17] A. Lucas-Consuegra, F. Dorado, C. Jiménez-Borja, J.L. Valverde, Appl. Catal. B: Environ. 78 (2008) 222.
[18] A. Lintanf, E. Djurado, P. Vernoux, Solid State Ionics 178 (2008) 1998.
[19] I. Salem, X. Courtois, E.C. Corbos, P. Marecot, D. Duprez, Catal. Commun. 9 (2008) 664.
[20] M. Casapu, J.-D. Grunwaldt, M. Maciejewski, F. Krumeich, A. Baiker, M. Wittrock, S. Eckhoff, Appl. Catal. B: Environ. 78 (2008) 288.
[21] Y. Hu, K. Griffiths, Appl. Surf. Sci. 254 (2008) 1666.
[22] J. Xiao, X. Li, S. Deng, F. Wang, L. Wang, Catal. Commun. 9 (2008) 563.
[23] X. Wang, A. Wang, X. Wang, X. Yang, T. Zhang, Gold Bull. 40 (2007) 52.
[24] N.W. Cant, N.J. Ossipoff, Catal. Today 36 (1997) 125.
[25] S. Qiu, R. Ohnishi, M. Ichikawa, J. Phys. Chem. 98 (1994) 271.
[26] S. Qiu, R. Ohnishi, M. Ichikawa, J. Chem. Soc., Chem. Commun. (1992) 1425.
[27] Y. Shi, H. Pan, Y. Zhang, W. Li, Catal. Commun. 9 (2008) 796.
[28] R. Zhang, S. Kaliaguine, Appl. Catal. B: Environ. 78 (2008) 275.
[29] S.P. Ramnani, S. Sabharwal, J.V. Kumar, K.H.P. Reddy, K.S.R. Rao, P.S.S. Prasad, Catal. Commun. 9 (2008) 756.
[30] J.R.H. Carucci, K. Arve, K. Eränen, D.Y. Murzin, T. Salmi, Catal. Today 133 (2008) 448.
[31] J.M.D. Cónsul, I. Costilla, C.E. Gigola, I.M. Baibich, Appl. Catal. A: Gen. 339 (2008) 151.
[32] J.M.D. Cónsul, C.A. Peralta, J.A.C. Ruiz, H.O. Pastore, I.M. Baibich, Catal. Today 133 (2008) 475.
[33] Y. Xue, G. Lu, Y. Guo, Y. Guo, Y. Wang, Z. Zhang, Appl. Catal. B: Environ. 79 (2008) 262.
[34] C. He, M. Paulus, W. Chu, J. Find, J.A. Nickl, K. Köhler, Catal. Today 131 (2008) 305.
[35] M.F. Irfan, J.H. Goo, S.D. Kim, Appl. Catal. B: Environ. 78 (2008) 267.
[36] E.B. Silveira, C.A.C. Perez, M.A.S. Baldanza, M. Schmal, Catal. Today 133 (2008) 555.
[37] Y. Shi, H. Pan, Z. Li, Y. Zhang, W. Li, Catal. Commun. 9 (2008) 1356.
[38] S. Roy, M.S. Hegde, Catal. Commun. 9 (2008) 811.
[39] S. Roy, B. Viswanath, M.S. Hegde, G. Madras, J. Phys. Chem. C 112 (2008) 6002.
[40] K. Asano, C. Ohnishi, S. Iwamoto, Y. Shioya, M. Inoue, Appl. Catal. B: Environ. 78 (2008) 242.
[41] F. Thibault-Starzyk, E. Seguin, S. Thomas, M. Daturi, H. Arnolds, D.A. King, Science 324 (2009) 1048.
[42] F. Solymosi, T. Bánsági, T.S. Zakar, Catal. Lett. 87 (2003) 7.
[43] F. Solymosi, T. Bánsági, T.S. Zakar, Phys. Chem. Chem. Phys. 5 (2003) 4724.
[44] M. Kantcheva, O. Samarskaya, L. Ilieva, G. Pantaleo, A.M. Venezia, D. Andreeva, Appl. Catal. B: Environ. 88 (2009) 113.
[45] M.A. Debeila, N.J. Coville, M.S. Scurrell, G.R. Hearne, Catal. Today 72 (2002) 79.
[46] M.A. Debeila, N.J. Coville, M.S. Scurrell, G.R. Hearne, M.J. Witcomb, J. Phys. Chem. B 108 (2004) 18254.
[47] M.A. Debeila, N.J. Coville, M.S. Scurrell, G.R. Hearne, Appl. Catal. A: Gen. 291 (2005) 98.
[48] M.A. Debeila, N.J. Coville, M.S. Scurrell, G.R. Hearne, J. Mol. Catal. A: Chem. 219 (2004) 131.
[49] Y. Wang, D. Zhang, Z. Yu, C. Liu, J. Phys. Chem. C 114 (2010) 2711.
[50] P. Bera, K.C. Patil, V. Jayaram, M.S. Hegde, G.N. Subbanna, J. Mater. Chem. 9 (1999) 1801.
[51] T. Fujitani, I. Nakamura, A. Takahashi, M. Haneda, H. Hamada, J. Catal. 253 (2008) 139.
[52] T.M. Salama, R. Ohnishi, M. Ichikawa, J. Chem. Soc., Faraday Trans. 92 (1996) 301.
[53] N. Macleod, R. Cropley, R.M. Lambert, Catal. Lett. 86 (2003) 69.
[54] J.Y. Lee, J. Schwank, J. Catal. 102 (1986) 207.
[55] C.P. Vinod, J.W.N. Hansa, B.E. Nieuwenhuys, Appl. Catal. A: Gen. 291 (2005) 93.
[56] J.L.C. Fajín, M.N.D.S. Cordeiro, J.R.B. Gomes, J. Phys. Chem. C 113 (2009) 8864.
[57] L. Ilieva, G. Pantaleo, J.W. Sobczak, I. Ivanov, A.M. Venezia, D. Andreeva, Appl. Catal. B: Environ. 76 (2007) 107.
[58] L. Ilieva, G. Pantaleo, R. Nedyalkova, J.W. Sobczak, W. Lisowski, M. Kantcheva, A.M. Venezia, D. Andreeva, Appl. Catal. B: Environ. 90 (2009) 286.
[59] B. Hammer, Faraday Discuss. 110 (1998) 323.
[60] B. Hammer, J. Catal. 199 (2001) 171.
[61] B. Hammer, Surf. Sci. 459 (2000) 323.
[62] Q. Ge, M. Neurock, J. Am. Chem. Soc. 126 (2004) 1551.
[63] S. González, D. Loffreda, P. Sautet, F. Illas, J. Phys. Chem. C 111 (2007) 11376.
[64] L. Olsson, V.P. Zhdanov, B. Kasemo, Surf. Sci. 529 (2003) 338.
[65] L. Olsson, B. Andersson, Top. Catal. 28 (2004) 89.
[66] H.A.C.M. Hendrickx, B.E. Nieuwenhuys, Surf. Sci. 175 (1986) 185.
[67] B.L.M. Hendriksen, M.D. Ackermann, R. van Rijn, D. Stoltz, I. Popa, O. Balmes, A. Resta, D. Wermeille, R. Felici, S. Ferrer, J.W.M. Frenken, Nature Chem. 2 (2010) 730.
[68] J.L.C. Fajín, M.N.D.S. Cordeiro, J.R.B. Gomes, J. Phys. Chem. C 111 (2007) 17311.
[69] J.L.C. Fajín, M.N.D.S. Cordeiro, J.R.B. Gomes, J. Phys. Chem. C 112 (2008) 17291.
[70] H. Sakurai, S. Tsubota, M. Haruta 102 (1993) 125.
[71] G. Kresse, J. Hafner, Phys. Rev. B 47 (1993) 558.
[72] G. Kresse, J. Furthmüller, Comput. Mater. Sci. 6 (1996) 15.
[73] G. Kresse, J. Furthmüller, Phys. Rev. B 54 (1996) 11169.
[74] J.P. Perdew, J.A. Chevary, S.H. Vosko, K.A. Jackson, M.R. Pederson, D.J. Singh, C. Fiolhais, Phys. Rev. B 46 (1992) 6671.
[75] P.E. Blöchl, Phys. Rev. B 50 (1994) 17953.
[76] G. Kresse, D. Joubert, Phys. Rev. B 59 (1999) 1758.
[77] H.J. Monkhorst, J.D. Pack, Phys. Rev. B 13 (1976) 5188.
[78] G. Henkelman, H. Jónsson, J. Chem. Phys. 111 (1999) 7010.
[79] K.J. Laidler, Chemical Kinetics, third ed., Harper Collins, New York, 1987, pp. 193.
[80] A.U. Nilekar, J. Greeley, M. Mavrikakis, Angew. Chem., Int. Ed. 45 (2006) 7046.
[81] J.L.C. Fajin, M.N.D.S. Cordeiro, J.R.B. Gomes, App. Catal. A: Gen. 379 (2010) 111.
[82] H. Huber, D. McIntosh, G.A. Ozin, Inorg. Chem. 16 (1977) 975.
[83] R. Liu, W. Shen, J. Zhang, M. Li, Appl. Surf. Sci. 254 (2008) 5706.
[84] Á. Logadóttir, J.K. Nørskov, J. Catal. 220 (2003) 273.
[85] K.C. Taylor, R.L. Klimisch, J. Catal. 30 (1973) 478.
[86] M. Shelef, H.S. Gandhi, Ind. Eng. Chem. Prod. Res. Develop. 11 (1) (1972).
[87] R.L. Klimisch, K.C. Taylor, Environ. Sci. Techn. 7 (1973) 127.
[88] J.L.C. Fajin, M.N.D.S. Cordeiro, J.R.B. Gomes, J. Mol. Struct.: Theochem. 946 (2010) 51.
[89] J.A. Rodríguez, J. Evans, J. Graciani, J.-B. Park, P. Liu, J. Hrbek, J.F. Sanz, J. Phys. Chem. C 113 (2009) 7364.
[90] S. Galvagno, G. Parravano, J. Catal. 55 (1978) 178.
[91] S.D. Ebbesen, B.L. Mojet, L. Lefferts, J. Phys. Chem. C 113 (2009) 2503.
[92] J. Siera, B.E. Nieuwenhuys, H. Hirano, T. Yamada, K.I. Tanaka, Catal. Lett. 3 (1989) 179.